Volume 4 Number 11 November 1977 **Nucleic Acids Research**

A low resolution model for the chromatin core particle by neutron scattering

Pedro Suau, G.Geoff Kneale, Gordon W.Braddock, John P.Baldwin and E.Morton Bradbury

Biophysics Laboratories, Portsmouth Polytechnic, St.Michael's Building, White Swan Road, Portsmouth, Hampshire, UK

Received 27 July 1977

ABSTRACT

Neutron scattering studies have been applied to chromatin core particles in solution, using the contrast variation technique. On the basis of the contrast dependance of the radius of gyration and the radial distribution function it is shown that the core particle consists of a core containing most of the histone around which is wound the DNA helix, following a path with a mean radius of 4.5 nm, in association with a small proportion of the histones. Separation of the shape from the internal structure, followed by model calculations shows that the overall shape of the particle is that of a flat cylinder with dimensions *ca.* 11x11x6 nm. Further details of the precise folding of the DNA cannot be deduced from the data, but detailed model calculations support concurrent results from crystallographic studies[25].

INTRODUCTION

It is now well-established that chromatin consists of a repeating subunit called the nucleosome[1-8]. In most animal tissues the nucleosome DNA repeat length is in the range 190 to 200 base pairs (b.p.). Exceptions to this are found for certain specialised cells e.g. erythrocytes 210 b.p.[9], 220 b.p.[10], sea urchin sperm 241 b.p.[11] etc. and also for lower eukaryotes [12-14]. In all cases, however, more prolonged nuclease digestion gave a well-defined subnucleosome particle called the 'core' particle[15] containing a precise length of DNA, nominally 140 b.p. and two each of the histones H2A, H2B, H3 and H4.

Studies have been carried out in parallel by several groups to establish the structure of the nucleosome and core particle. Neutron scatter studies of nucleosomes[10,16,17] and core particles[18] established that DNA was on the outside of the particle and was highly hydrated. An early neutron diffraction study[19] of chromatin as a function of concentration and contrast suggested that the DNA regions hydrated preferentially to the protein regions and that protein regions were contrasted against a hydrated DNA matrix. Many studies have suggested that the nucleosome had a spherical structure, although from

a dark field scanning electron microscope study[20,21] it has been proposed that the nucleosome is disc shaped 13.5x13.5x5 nm with a loop, or loops, of DNA around the periphery of the disc. The calculated scatter curve from this type of model has been found to give good agreement with the experimental scatter from core particles in D_2O[22]. More detailed studies of nucleosomes using the contrast variation technique of Stuhrmann[23] have established a set of basic scattering functions enabling the contributions from the shape and internal structure to be separated[10]. It was proposed that a DNA rich region surrounded a protein core of 3.2 nm radius. Although a simple ellipsoidal model with axial ratio close to 0.5 fitted the data best, models closer to a spherical shape could not at that point be ruled out.

We now report a more extensive analysis on chromatin core particles, including calculations of the radial distribution function which gives the maximum dimensions of the particle. Furthermore, computer programmes have been developed for the simulation of scatter curves from a wide variety of three dimensional models. Although in general a unique structure cannot be derived from the spherically averaged intensities obtained by solution scattering techniques[23] in certain favourable cases much of the ambiguity can be removed if certain simplifying assumptions are made. We show below that this is the case for our study where, assuming DNA is present in the B form the overall structure of the core particle is severely constrained by our data. Despite these restrictions variations on such a model are possible and these have been tested by detailed model calculations.

During the course of this analysis an independent study[25] of the core particle by X-ray crystallography and electron microscopy has been performed. This study establishes the shape of the core particle in the crystal and the neutron scatter study described here shows that the solution structure is very similar to the crystal structure.

The contrast variation method

The method of contrast variation has been developed by several authors [23,26,27] and applications of the method have recently been reviewed[24,28]. It can be summarised as follows:

The measurement of the small angle scattering in solvents of different scattering length densities allows the separation of the contributions of the shape and internal structure to the scattering curves. The excess scattering length density of a particle in solution can be described as being composed of two parts:

$$\rho(\vec{r}) = \bar{\rho}\Omega_F(\vec{r}) + \rho_S(\vec{r}) \quad (1)$$

where $\bar{\rho}$ is the contrast or mean excess scattering length density given by $\bar{\rho} = \rho_{mean} - \rho_{solvent}$, i.e. the difference between the mean scattering length density of the solute and the scattering length density of the solvent. $\Omega_F(\vec{r})$ is a function that is unity inside the regions of the molecule that are inaccessible to the solvent and zero elsewhere. $\rho_S(\vec{r})$ represents the fluctuations of the scattering length density about ρ_{mean}.

The scattering amplitude is given by

$$A(\vec{s}) = \bar{\rho}A_F(\vec{s}) + A_S(\vec{s}) \quad (2)$$

where $s = 2 \sin\theta/\lambda$ (2θ is the scattering angle and λ the wavelength). The scattering intensity is obtained by squaring the amplitudes and averaging with respect to solid angle[29]

$$I(\vec{s}) = \langle | A(\vec{s}) |^2 \rangle = \bar{\rho}^2 I_C(s) + \bar{\rho} I_{CS}(s) + I_S(s) \quad (3)$$

thus the scattering can be decomposed into three basic scattering functions. $I_S(s)$ will be observed at vanishing contrast, i.e. when the mean scattering length density of the solute is matched by the scattering length density of the solvent. $I_F(s)$ is the extrapolated intensity to infinite contrast where the fluctuations of scattering length density about ρ_{mean} can be neglected and only the shape contributes to the scattering.

In the case of neutron scattering in H_2O/D_2O mixtures the influence of the exchange of labile protons is taken into account by introducing a quantity $\Omega_C(\vec{r}) = \Omega_F(\vec{r}) - \Omega_E(\vec{r})$ in place of $\Omega_F(\vec{r})$: $\Omega_E(\vec{r})$ describes the distribution of exchangeable sites within the particle. $\rho(\vec{r})$ will increase as the solvent scattering length density is decreased, except at the exchangeable sites where $\rho(\vec{r})$ will decrease. The rigorous definition of these quantities is given by Ibel and Stuhrmann[29].

At atomic resolution $\Omega_C(\vec{r})$ is always one inside the particle except at exchangeable proton sites. However for low resolution model calculations one may consider a particle to have an effective $\Omega_C(\vec{r})$ corresponding to averaging scattering densities over rather large regions. This effective $\Omega_C(\vec{r})$ of particles penetrable by solvent can be considerably less than one and will only approach one in the regions of the molecule inaccessible to solvent.

Neutron scattering in H_2O/D_2O mixtures measures in effect the 'dry' particles. Water (i.e. a mixture of D_2O and H_2O solvent) under appropriate buffer conditions usually penetrates to all regions outside the van der Waals envelopes of the atoms in a particle and its bound water. Any regions which are impenetrable to the solvent are part of the particle so that $\Omega_C(\vec{r})$ is

non zero in such regions. The bound water in a particle is usually able to exchange with the solvent so that if the solvent is a pure H_2O/D_2O mixture the bound water scatters exactly like the solvent. Thus in the region of the bound water, $\Omega_E(\vec{r}) = 1$ and $\Omega_C(\vec{r}) = 0$[24].

EXPERIMENTAL PROCEDURES

Nuclei preparation and digestion

Chicken erythrocyte nuclei were isolated by the method of Murray et al[30] the preparation began 1-2 hours after killing. After the final centrifugation the nuclei concentration was adjusted at 2×10^9 nuclei/ml. Digestion with micrococcal nuclease (Microbiological Research Establishment, Porton, Salisbury, England) was carried out at 37°C with 400u of nuclease per ml in 0.25 M sucrose, 10 mM Tris-ClH 0.1 mM $CaCl_2$, pH 7.6. Digestion was stopped by making the solution 10 mM EDTA and cooling on ice. After centrifugation at 15000 x g for 15 mins. the nuclei were burst by dialysis against 2 mM EDTA 10 mM Tris HCl, pH 8. The nuclear debries were pelleted and the supernatant made 0.35% sucrose.

Digestion products were fractionated by zonal centrifugation over a 5-30% sucrose gradient in 2 mM EDTA, 10 mM Tris-HCl, pH 8.

Characterisation of the subunits

Acid soluble proteins were analysed by acrylamide gel electrophoresis according to the method of Panyim and Chalkley[31]. Figure 1 shows that purified core particles contain very little H1 and H5 but a full complement of the other four histones[32].

DNA fragments were purified by phenol extraction after sucrose digestion in 0.14 M NaCl 1 mM EDTA, 10 mM Tris HCl, pH 7.6. DNA samples were run on 7% acrylamide gels according to the method of Maniatis[33]. The gels were calibrated with restriction enzyme fragments from λdv 1Bsu DNA (provided by Professor H G Zachau). Gels were stained for 1 hour with ethidium bromide at 1 µg/ml in 1 mM EDTA pH 7.6 at 4°C.

The core particle band appears to consist of a narrow band of about 137 base pairs with smaller components of about 155 and 120 base pairs (Figure 1) giving an overall polydispersity in molecular weight below 5%. Analysis of this DNA on formamide denaturing gels[34] did not show any single stranded nicks. Analytical centrifugation gave $S_{w,20} = 11.1$, in agreement with Shaw et al.[32].

Neutron measurements

The neutron experiments were carried out at the small angle scattering

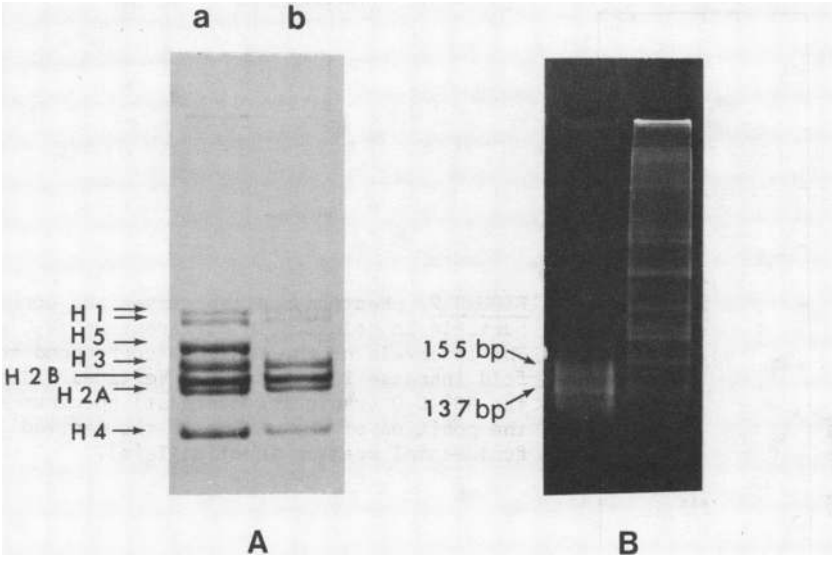

FIGURE 1 Polyacrylamide gel electrophoresis of DNA and acid soluble proteins from purified core particles prepared by micrococcal nuclease digestion of chicken erythrocyte nuclei. A) a - histones extracted from chicken nuclei; b - histones from the purified monomer fractions. B) Calibration of the DNA component of purified monomer with λdv lBsu fragments.

apparatus D11[35,36] of the Institute Max von Laue-Paul Langevin, Grenoble. Neutrons from the high flux reactor were moderated by the liquid deuterium (cold source). Neutrons were monochromatized by a helical slot velocity selector giving a mean wavelength of 0.83 nm with full half-width of 8%. The scattered neutrons were detected by a BF_3 ionisation chamber consisting of 4096 individual counters. The samples in quartz cells of 1 or 2 mm thickness were measured at two camera settings of 2.5 and 0.84 m. The data were scaled using the overlapping regions and merged to obtain the complete scattering curve (Figure 2). The data were not corrected for distortions due to wavelength distribution. Variations of detector response were corrected by division by the water spectrum after a small correction for the cell scatter.

RESULTS AND DISCUSSION

Absolute intensities

The intensity of coherent neutron scattering into solid angle $\Delta\Omega$ is given by:

$$I_S(s) = \Phi_S(\frac{d\sigma}{d\Omega})_S \Delta\Omega \, n_t \, T_S \qquad (4)$$

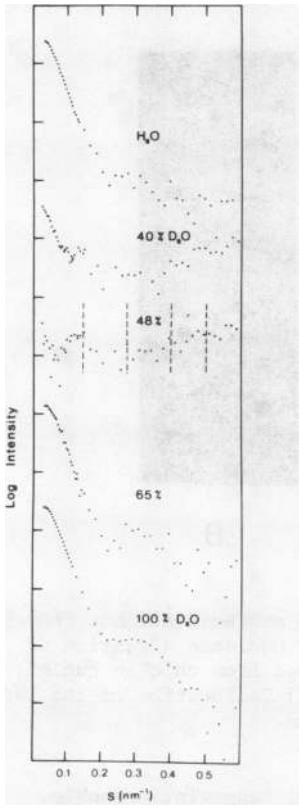

FIGURE 2 Neutron scatter curves per core particle in solution in different D_2O/H_2O mixtures. The intervals of the ordinate correspond to a 10 fold increase in intensity. Vertical lines on the 48% D_2O (vanishing contrast) spectrum show the position of the maxima of the derived fundamental scatter function $I_S(s)$.

where Φ is the incident flux and T_S the transmission.

In order to calculate the differential scattering cross section per particle we need to determine a) the number of particles contributing to the scatter, and b) the absolute intensity of scattered neutrons per unit flux. The former is calculated by biochemical measurements of the DNA component and the latter by reference to the incoherent scatter from water. The incoherent water scatter (neglecting any variation with scattering angle from multiple scattering) is given by:

$$I_w(s) = \Phi_w . A \frac{\Delta\Omega}{4\pi} (1-T_w) \quad (5)$$

where A is the sample area. Subsequent division of the two spectra (normalised for flux and transmission) gives:

$$\frac{I_S/T_S\Phi_S}{I_w/\Phi_w} = \frac{C.D}{1-T_w} \cdot \frac{4\pi N}{M} \cdot \left(\frac{d\sigma}{d\Omega}\right)_S \quad (6)$$

where n_t = N.A.D.C/M (N is Avagadro's number, D the thickness of the sample, and C/M is the ratio of the concentration of molecular weight of any given

component in the particle). In this case the concentration and molecular weight are readily obtainable for the DNA component (see experimental details) and equation (6) may be used to obtain $(d\sigma/d\Omega)_S$ for the core particles.

Zero-angle scattering

The zero-angle scatter is given by extrapolation of low angle scattering to zero-angle using Guinier's plot[37] (Figure 3). The interparticle effect often seen between the charged particles has been minimised by finding the best buffer conditions. The square root of the intensity at zero-angle of a dilute monodisperse solution is proportional to the contrast $\bar{\rho}$. The results of Figure 4 confirm that $\sqrt{I(o)}$ depends linearly on the solvent scattering length density. The intercept of the straight line on the abcissa gives the mean scattering length density of the solute, ρ_{mean}. For chicken erythrocyte core particle it equals $(2.78 \pm 0.01) \times 10^{10}$ cm^{-2}, corresponding to 48% D_2O. The mean scattering length for the particle is then equal to that of the solvent. As expected, the value is smaller than that found for chicken erythrocyte nucleosomes (with 195 ± 40 b.p.) of $(2.97 \pm 0.01) \times 10^{10}$ cm^{-2} [10], and slightly lower than the one reported by Pardon et al.[18] (also for chicken erythrocyte core particles) of 2.85×10^{10} cm^{-2}.

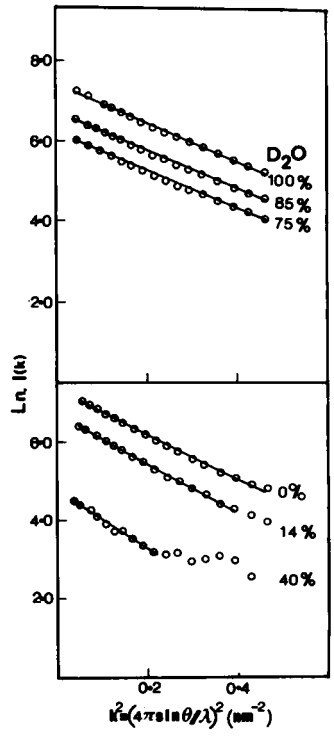

FIGURE 3 Guinier plots for core particles in solution at a concentration of 10 mg/ml in different D_2O/H_2O mixtures.

If both composition and number of exchangeable protons were known, V_F, the volume of the dry particle included in the van der Waals envelopes could be obtained as $V_F = \sum_i b_i/\rho_{mean}$. We have assumed 140 b.p. of DNA and a pair of each of the four histones to calculate the number of exchangeables. The results of infrared spectroscopy[38] show that all labile protons in chromatin are exchangeable with the exceptions of about 40% of the protons of the amide groups. Taking into account partial deuteration, out of a total of 2260 labile protons about 1085 will on average exchange in the particle at the contrast match position and of these only 269 are DNA protons. We obtain $V_F = 223\ nm^3$. This gives excellent agreement with the volume calculated from the partial specific volumes of DNA and the component amino acid residues of $218\ nm^3$.

When the intensities are put on an absolute scale in terms of $(d\sigma/d\Omega)(s)$ the slope of the straight line, Figure 4, gives the apparent volume $V_C = 186\ nm^3$. $V_C(\int\Omega_C(r)d\tau)$ is equal to $V_F - V_E = (1-\bar{\Omega}_E)\ V_F : V_E(\int\Omega_E(r)d\tau)$ can be shown to be related to the number of the exchangeable protons by the factor $(b_D - b_H)/(\rho_{D_2O} - \rho_{H_2O})$. We estimated $V_E = 34\ nm^3$ (40% of the labile protons assumed not to exchange); thus $V_F = V_C + V_E = 220\ nm^3$ in agreement with the above calculations. $(1-\bar{\Omega}_E)$ can be regarded as a loss factor due to H/D exchange. $\bar{\Omega}_E = 0.15$ is found for core particles (compared to 0.2 for myoglobin in D_2O/H_2O mixtures)[29].

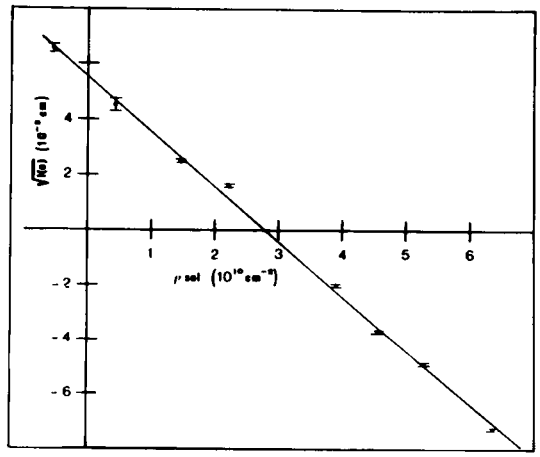

FIGURE 4 Variation of the intensity at zero-angle against solvent scattering length density. I(o) was found by extrapolation of the small angle scattering using Guinier plots.

Contrast variation of the radius of gyration

The radius of gyration, Rg, of the core particles was measured for eight different D_2O/H_2O mixtures using the Guinier approximation[37]. The plot ln I(s) against K^2 (= $4\pi^2 s^2$) gave linear plots (Figure 3) with regression coefficients > 0.95. We found the approximation to be valid when s < 0.02 nm. The variation of the radius of gyration with contrast has been analysed with the equation:

$$Rg^2 = R_C^2 + \alpha/\bar{\rho} - \beta/\bar{\rho}^2 \qquad (7)$$

From a plot of the Rg^2 against the reciprocal of the contrast $1/\bar{\rho}$ (Figure 5) the parameters R_C, α and β were determined. At infinite contrast ($1/\bar{\rho} = 0$) we obtain the radius of gyration, R_C of the shape function $\Omega_C(r)$. Details of the internal structure do not contribute to the scattered intensity when the contrast tends to infinity and the effect of fluctuations of $\Omega_E(r)$ about the mean is small, so R_C closely corresponds to the radius of gyration of the volume occupied by the particle in solution. R_C was found to be 3.94 ± 0.05 nm. This is slightly smaller than the value found for chicken erythrocyte nucleosomes as expected. The value determined by Pardon et al.[18] of 4.11 nm is higher than both values we have found.

The coefficients α and β give information on the internal structure of the particle. The relation of these coefficients to the particle structure

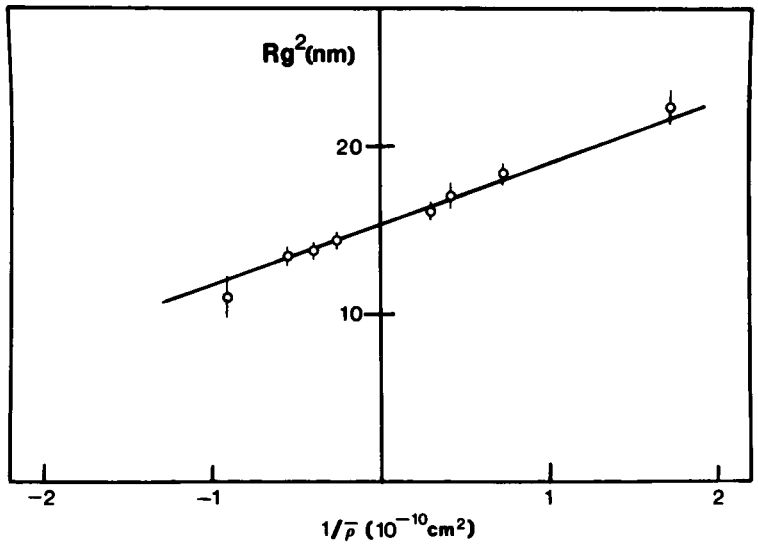

FIGURE 5 Variation of Rg^2 of core particles as a function of the reciprocal contrast. Standard deviations are shown for each point, calculated from the regression analysis.

have been given by Ibel and Stuhrmann[29] as:

$$\alpha = (m_S^{(2)}/V_C) - 2\vec{m}_E^{(1)}.\vec{m}_S^{(1)}/V_C^2 \quad (8)$$

and

$$\beta = (m_S^{(1)})^2/V_C^2 \quad (9)$$

where $m_S^{(1)} = \int\rho_S(\vec{r})r d\tau$, the first moment of the internal structure function and $m_S^{(2)} = \int\rho(\vec{r})r^2 d\tau$, the second moment.

The positive sign of the tangent $\alpha = (3.6 \pm 0.4) \times 10^{-4}$ reflects a feature common to many globular proteins, the location of the stronger scattering components on the outside of the particle, in our case the DNA component[23].

We have calculated that the second term of equation (8) is very small compared to the first term, allowing the second moment of the internal structure function $m_S(2)$ to be calculated from α and the value of V_C. We obtain $m_S^{(2)} = 7 \times 10^{-2}$ nm^3. This is lower than the value found for nucleosomes (195 ± 40 b.p.) of 9.7×10^{-2} nm^3.

The value of β is close to zero within an estimated error of 1.1×10^{-9} nm^{-2}. From this we estimate the separation between the centres of scattering masses of the protein and DNA to be less than 10 Å.

Basic scattering functions

The basic scattering functions were obtained from the experimental curves in different D_2O/H_2O mixtures by parabolic regression using equation(4). An advantage of analysing the scattering results in terms of basic scattering functions consists of the separation of shape and internal structure contributions. The regression process also allows an important part of the statistical noise to be eliminated.

The internal structure function $I_S(s)$

The internal structure function $I_S(s)$ is plotted in Figure 6. It shows characteristics of a two-level step function and has a strong peak at about 7.4 nm equivalent spacing and subsidiary maxima at about 3.6, 2.6 and 2.1 nm. The experimental scattering curve at the contrast matched position should be equivalent to $I_S(s)$ because when $\rho_{sol} = \rho_{mean}$, $\Omega_C(\vec{r})$ does not contribute to the scattered intensity. This is the 48% D_2O scatter curve of Figure 2.

The basic scattering function $I_{CS}(s)$

The basic scattering function $I_{CS}(s)$ correlates shape and internal structure of the particle (equation (3)). At low angle the $I_{CS}(s)$ term is dominated by the spherically averaged structure[39]. This means in practice that the fine details of $\Omega_C(\vec{r})$ and $\rho_S(\vec{r})$ are not correlated. $I_{CS}(s)$ is

negative below 0.17 nm^{-1} (Figure 6). $A_S(\vec{s})$ must also be negative in this region since it is determined by positive value of α. At $s = 0.17\ nm^{-1}$ the function $I_{CS}(\vec{s})$ reaches zero. Thus the spherically averaged parts of $A_C(\vec{s})$ and/or $A_S(\vec{s})$ are changing sign. It is reasonable to assume that it is the spherical part of $I_C(s)$ that goes to zero, as $I_S(s)$ has a maximum in this region.

The shape function $I_C(s)$

The function $I_C(s)$ corresponds to the scattering that would be observed at infinite contrast where there is no contribution from the internal structure $\rho_S(s)$ and only a small contribution from the internal structure of $\Omega_E(\vec{r})$ is present.

The shape transform for core particles does not show maxima at 10.0 nm and 5.5 nm typical of fibre diffraction diagrams (Figure 6). There is a plateau around .27 nm^{-1} that appears to be split into two components at .3 nm^{-1} and 0.24 - 0.25 nm^{-1}. A secondary maximum at about 0.48 nm^{-1} can also be observed in the shape function and also in the 100% D_2O spectrum.

In studies of contrast variation of proteins $\Omega_C(\vec{r})$ can be considered to be uniform when the small influences from H/D exchange are neglected. In many cases this appears to be a fairly good approximation, even if the predominantly surface location of the polar and charged residues of the molecule makes the effective $\Omega_C(\vec{r})$ fall gradually at the periphery. Nucleosomes could be an extreme case of this type. With the limited amount of DNA per nucleosome and its outside location the function $\Omega_C(\vec{r})$ could fall rather abruptly at the edge of the DNA region. This DNA region would be highly accessible to solvent. Low- angle neutron scattering contrast variation with sucrose and glycerol of core particles in solution indicate that the volume of the particle which is accessible to small molecules is much smaller than the volume accessible to water[40]. This shows that a large amount of bound or occluded water is associated with the particle. The radius of gyration of the shape function R_C, corresponds to a sphere of uniform density of 5.2 nm radius. However, the volume of such a sphere (590 nm^3) would be more than twice V_P(223 nm^3). To get such a volume with close packing of the components an ellipsoid would have an axial ratio of about 4 which contradicts the experimental data[10].

The distribution function

Just as a Patterson function is calculated from the observed diffraction intensities from crystals, so a function D(r) may be calculated from solution scattered intensities. D(r) is the spherical average of the Patterson

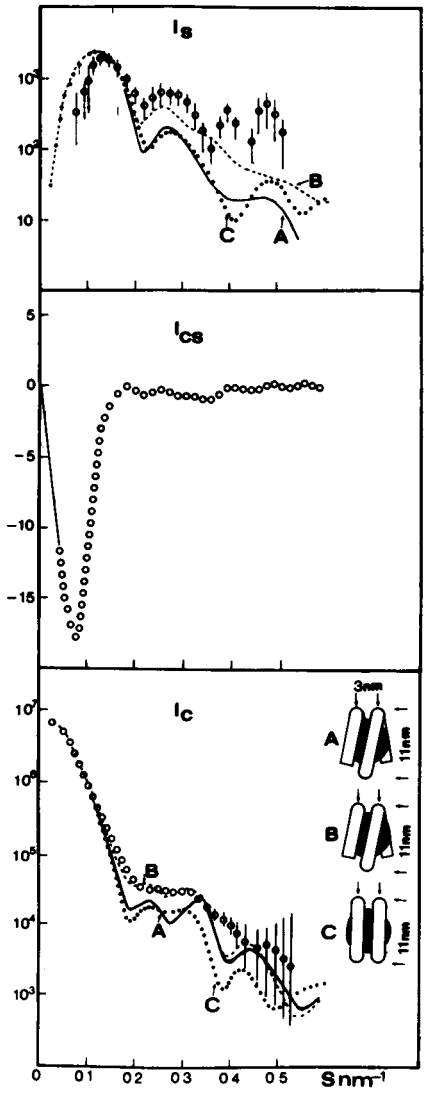

FIGURE 6 The fundamental scatter functions (arbitrary units). The calculated curves from the three models A, B, and C are fitted to the experimental curves.(O). The models are as follows:
A regular helix around the histone core.
B irregular helix, constrained to follow the surface of the histone core.
C two parallel DNA rich rings around the core.
The best fits were found with a protein core approximately 6.6 x 6.6 x 6.0 nm and a DNA coil, in association with some of the proteins, having a pitch of 3.0 nm (3.5 nm for model C).
The weightings of the DNA rich regions to protein core were in the ratio 0.6:1 for $I_C(s)$.

function of a particle ($\langle \rho(r) * \rho(r) \rangle$) integrated over a spherical surface of area $4\pi r^2$ to give a one dimensional representation[24]. D(r) is given by:

$$D(r)=8\pi r/sI(s) \sin(2\pi rs)ds.$$

$D_C(r)$ calculated from $I_C(s)$ is shown in Figure 7. The D(r) function extends to a value of about 11.0 nm corresponding to the maximum dimension of the particle. This important parameter has been used as a constraint in

the model calculations. The maximum of the distribution (at 4.4 nm) is displaced towards the low side of the distribution of distances expected for a sphere having the same radius as the particle. Both anistropy of the molecular dimensions and a highly convoluted outside surface of the particle can lead to this effect.

Model calculations

The following types of models have been studied in a systematic manner:

1) Spherical models with a spherical histone core and an outer shell of hydrated DNA.

2) 'Baseball' models where the DNA follows a path around a histone core similar to the seam on a baseball.

3) Disc shaped models, oblate ellipsoids with a spherical histone core and the DNA located in an annulus around the core.

4) Disc shaped models where the DNA is confined to two rings around a spherical or oblate spheroid histone core (Figure 6C).

5) As 4 with the DNA following a regular helix around the histone core (Figure 6A).

6) As 5 with the DNA coil distorted so as to maintain contact with the protein core (Figure 6B).

It was shown in the earlier paper on nucleosomes[10] that an oblate spheroid of axial ratio 0.5 gave the best fit to the low angle region of the

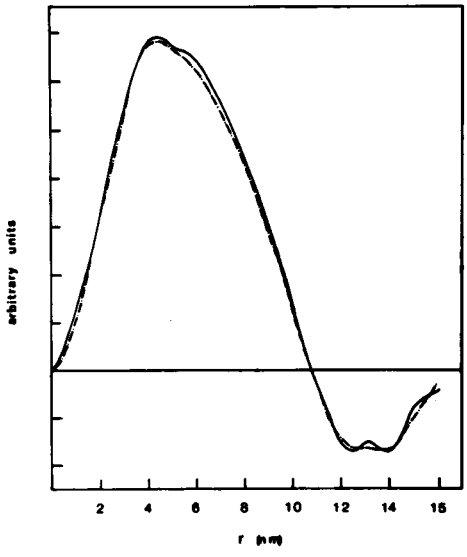

FIGURE 7 Distance distribution function D(r) derived from the shape function $I_C(s)$. The errors have been propagated through the transformation to give $I_C(s) + \Delta$ (short line) and $I_C(s) - \Delta$ (dashed line).

I_C curve and this is also the case for core particles. Spherical models and 'baseball' models have been excluded because of the very poor fit they gave to I_C even at low angles. Oblate ellipsoid models for core particles gave good fits to I_C at low angles and various configurations of histone and DNA in this type of model, as described in 3-6 above, have been tried to obtain the best fit for the full I_C curve. We have used the following information from the D(r) function and the radius of gyration analysis to define the limits of our model.

1) From the D(r) function, the maximum dimensions of the particle must be close to 11 nm.

2) The radius of gyration at 40% D_2O (4.7 ± 0.2) will approximate to that of the DNA component. This value is lower than that found previously for core particles[18,22]. Using also the maximum dimension of the particle, simple calculations show that to fit these parameters, the outer surface of the DNA helix must be located at the maximum radius of the particle. The DNA cannot pass through the central core, and the DNA must follow a path with a radius close to 4.5 nm. It should be noted that if the experimental Rg for DNA were appreciably smaller than 4.7 nm, the radius of the DNA could not be defined in this way.

3) The radius of gyration at 65% D_2O (3.5 ± 0.2 nm) will approximate to that of the histone. That value is higher than previously reported for core particles[18,22]. It is in agreement with a proportion (around 25%) of the protein existing in the outer DNA-rich regions, but with most of the protein occupying the central core.

Further limitations on the shape are imposed by the parameters R_C and V_C. All the above parameters place considerable constraints on acceptable structures for the core particles. The calculation of the scattering curves from a large number of models consistent with the above parameters indicate that the structure must have the form of an oblate ellipsoid with axial ratio close to 0.5. Thus from the maximum particle dimension (11 nm), the dimensions cannot vary appreciably from 11 x 11 x 5.5 nm.

The DNA is composed of 140 (± 20) b.p. corresponding to a length of 48 ± 7 nm (B form double helix). To give the observed Rg for DNA this length must be wound around the circumference of the disc-shaped particle following a path of *ca.* 4.5 nm radius, putting the length of one turn at 28 nm. Thus we calculate that 1.7 (± .2) turns of DNA would be required.

Now the overall organisation of the particle is established, the precise details of the structure can only be approached by trial and error

calculations on model calculations within this framework. However, the constraints on the structure are quite stringent. For instance with almost two turns of DNA and a particle thickness of 6 nm, the spacing between two turns of DNA can only vary from 0 to 2 nm (i.e. for a regular helix a pitch of 2-4 nm).

Fitting the I_C curve

The three models which gave the best fit so far to the I_C curve are illustrated in Figure 6. These correspond to models of types 4, 5 and 6 described earlier. Models of type 3 in which a single annulus of DNA surrounds a spherical histone core gave a computed scatter curve which deviated substantially from the I_C curve at s values above 0.1. As can be seen in Figure 6 the models with a coil of DNA around a histone core, similar to the model proposed by Finch et al.[25], gave a better fit to I_C than the model with DNA confined to two separated rings. An improved fit was obtained if the DNA was distorted to remain in contact with the histone core rather than a uniform coil The shape of the histone core in each of models 4, 5 and 6 was slightly oblate with axial ratios in the range 0.8 to 0.9. The pitch of the DNA coil was varied between 3 and 4 nm. The 3 nm pitch gave the best fit to the I_C curve.

Fitting the I_S curve

The I_S curve consists of well-defined maxima at 7.4 and 3.6 nm with poorly defined maxima indicated at 2.6 and 2.1 nm. In earlier calculations[10] it was found that the positions of the first and second maxima could be closely approximated by 2 step spherical models consisting of a histone core and a concentric shell of hydrated DNA. The position of the first maximum in I_S is mainly influenced by the outside dimensions of the particle while the second maximum is influenced by the dimensions of the protein core. Note that in the experimental scatter curve at 65% D_2O when protein dominates the scatter only the second maximum is seen. Thus the first two maxima could be explained in principle by these simple models. However, the outside dimension which gave the best fit to the first maximum was in the range 9.0 to 9.6 nm compared to the maximum dimension from the D(r) function of 11.0.

Figure 6 shows the calculated I_S curves for the three models and the experimental I_S curve. For all three models the position of the first maximum at 8.0 nm is higher than the experimental value of 7.4 nm. Complete agreement between the positions of these maxima could be obtained if the outer dimensions of the models were reduced. However, we are reluctant to

do this because the errors in the experimental I_S curve are very much higher than for the I_C curve. This is particularly so at low s values where I_C dominates the scatter. In spite of the experimental errors there is reasonable agreement between the calculated and experimental curves. Also in the 48% D_2O curve, Figure 2, the maximum is at 8.0 nm. As can be seen the calculated I_S curves even for very similar models can be distinguished above 0.2 nm. At the moment the errors at higher angles do not allow a definite choice to be made between these models although it is encouraging that the curve for model B agrees more closely with the 'experimental I_S, as found for I_C.

CONCLUSIONS

The values of the parameters derived from neutron small-angle scattering for nucleosomes (200 b.p.)[10] and for core particles both from chicken erythrocyte nuclei are very similar[42]. Although the nucleosome values are slightly larger than for core particles, these differences constitute a check on the consistency of both sets of data for they can be easily explained by the different amounts of DNA in the two particles.

The improved monodispersity of the core particles in comparison with nucleosomes has led to better data extending the scope of the model calculations and yielding new information on the particles. Model calculations have allowed us to explain the experimental data to a large extent and also to associate in a simple structure all the experimental parameters and the contrast behaviour of the scattering curves. Although it is not possible to find a unique solution for the shape of the particle the essential features of the low resolution structure can be proposed with some confidence as a result of this study.

a) The scattering of nucleosomes in solution is dominated by a protein core relatively inaccessible to water, which is surrounded by a hydrated DNA rich region of lower density.

b) The features of the basic internal structure function $I_S(\vec{s})$ indicate a clear separation in the particle of two regions of different scattering length density.

c) The contrast variation of Rg, coupled with a maximum dimension of 11 nm constrain the DNA to follow an approximately circular path with radius 4.5 nm.

d) The details of the shape function are best explained by a particle of about 0.5 axial ratio (11 x 11 x 5.5 nm) and with one and two thirds turns of DNA organised at 4.5 nm radius in a regular or maybe distorted helix of pitch 3.0 nm. Outside shape convolution as a result of the folding of the

DNA would not contribute noticeably to the scattering curve at low resolution if the DNA turns were 3.0 nm or less apart.

The details of the precise arrangement of the DNA around the core will ultimately come from complete three-dimensional crystal structure analysis. Preliminary reports[25] favour models of type A with a regular helix of pitch 2.8 nm, although more irregular structures can not be ruled out. It is encouraging to note that the results from neutron scattering solution studies (which deal with spherically averaged intensities) and those of an X-ray diffraction/electron microscopy analysis[25] (in which the protein and DNA cannot be distinguished) converge on the same low-resolution structure for the core particle. It would therefore appear that the solution and crystal structures are closely similar.

ACKNOWLEDGEMENTS

We are most grateful to Dr K Ibel for his generous assistance and advice on neutron scattering measurements, and to R P Hjelm, B G Carpenter and J K Simpson for discussion. We are grateful for computing advice from Dr M Johnson of the Rutherford Laboratory, U.K. and for use of computing facilities at this Laboratory. This work was supported by the Science Research Council (U.K.). P S has been supported by an EMBO Fellowship.

REFERENCES

1. Hewish D R and Burgoyne A L (1973) Biochem. Biophys. Res. Comm. 52, 504-510.
2. Rill R and Van Holde K E (1973) J. Biol. Chem. 248, 1080.
3. Olins A L and Olins D E (1973) J. Cell. Biol. 59, 252
4. Woodcock C L F (1973) J. Cell Biol. 59, 368
5. Kornberg R D and Thomas J O (1974) Science 184, 865
6. Kornberg R D (1974) Science 184, 868-871.
7. Noll M (1974) Nature 251, 249-251.
8. Oudet P, Gross-Bellard M and Chambon P (1975) Cell 4, 281
9. Morris N R (1976) Cell 9, 627
10. Hjelm R P, Kneale G G, Suau P, Baldwin J P, Bradbury E M and Ibel K (1977) Cell 10, 139-151.
11. Spadafora C, Bellard M, Compton J L and Chambon P (1976) FEBS Lett. 58, 353
12. Noll M (1976) Cell 8, 349-355.
13. Morris N R (1976) Cell 8, 357-363.
14. Johnson E M, Littau V C, Allfrey V G, Bradbury E M and Matthews (1976) Nucl. Acids Res. 3, 3313-3329.
15. Van Holde K E and Isenberg I (1975) Acc. Chem. Res. 8, 327
16. Bradbury E M, Baldwin J P, Carpenter B G, Hjelm R P, Hancock R and Ibel K (1975) Brookhaven Symposia in Biology No. 27, pIV 97
17. Bradbury E M, Hjelm R P, Carpenter B G, Baldwin J P and Kneale G G (1977) In 'Nucleic Acid - Protein Recognition'. Academic Press p.117
18. Pardon J F, Worcester D L, Wooley J C, Tatchell K, Van Holde K E and Richards B M (1975) Nucl. Acid Res. 2, 2163-2176.

19. Baldwin J P, Boseley P G, Bradbury E M and Ibel K (1975) Nature 253, 245
20. Langmore J P and Wooley J C (1974) J. Cell Biol. 63, 185a.
21. Langmore J P and Wooley J C (1975) Proc. Nat. Acad. Sci. USA 72, 2691
22. Richards B M, Pardon J F, Lilley D, Cotter R and Wooley J C (1977) Cell Biol. Int. Rep. 1, 107
23. Stuhrmann H B (1974) J. Appl. Cryst. 7, 173
24. Kneale G G, Baldwin J P and Bradbury E M (1977) Quarterly Rev. Biophys. In press.
25. Finch J T, Lutter L C, Rhodes D, Brown R S, Rushton B, Lewitt M and Klug A (1977) Nature 269, 29
26. Luzzati V, Tardieu A, Mateu L, Sardet C, Stuhrmann H B, Aggerbeck L and Scanu A M (1975) Brookhaven Symposia in Biology No. 27, pp IV 61-77.
27. Stuhrmann H B (1975) Brookhaven Symposia in Biology No. 27, pp IV 3-19.
28. Hjelm R P, Baldwin J P and Bradbury E M (1977) Methods in Cell Biology, 16, G Stein and J Stein eds. Academic Press, New York. In press.
29. Ibel K and Stuhrmann H B (1975) J. Mol. Biol. 93, 255
30. Murray K, Vidali G and Neelin J M (1968) Biochem. J. 107, 207
31. Panyim S and Chalkley R (1970) Biochim. Biophys. Acta 214, 216
32. Shaw B R, Herman T M, Kovacic R T, Baeuchaeu G S and Van Holde K E (1976) Proc. Nat. Acad. Sci. USA 73, 505
33. Maniatis T, Jeffrey A and Van de Sande H (1975) Biochemistry 14, 3784
34. Staynof D Z, Pinder J C and Gratzer W B (1974) Nature New Biol. 72, 235
35. Schmatz W, Springer T, Shelten J and Ibel K (1974) J. Appl. Cryst. 7, 96
36. Ibel K (1976) J. Appl. Cryst. 9, 630
37. Guinier A and Fournet G (1955) Small Angle Scattering of X-rays' Wiley and Sons (New York).
38. Bradbury E M, Price W C, Wilkinson G R and Zubay G (1962) J. Mol. Biol. 4, 50
39. Stuhrmann H B and Fuess H (1976) Acta Cryst. 32, 67
40. Baldwin J P, Kneale G G, Suau P, Braddock G W and Bradbury E M (1977) Manuscript in preparation.
41. Suau P (1977) Communicated at the 'Workshop on Small Angle Scattering of X-rays and Neutrons in Biology'. Villard de Lans.
42. Bradbury E M, Moss T, Hayashi H, Hjelm R P, Suau P, Stephens R M, Baldwin J P and Crane-Robinson C (1977) Cold Spring Spring Harbor Symposium. In press.